Journal of Fluids and Structures 32 (2012) 52–64

Contents lists available at ScienceDirect

Journal of Fluids and Structures

journal homepage: www.elsevier.com/locate/jfs

Mono- and multi-frequency vortex-induced vibrations of a long tensioned beam in shear flow

Rémi Bourguet [a,*], Didier Lucor [b], Michael S. Triantafyllou [a]

[a] Department of Mechanical Engineering, Massachusetts Institute of Technology, Cambridge, MA 02139, USA
[b] Institut Jean le Rond d'Alembert, UPMC Université Paris 06, 75252 Paris Cedex 05, France

ARTICLE INFO

Article history:
Received 29 October 2010
Received in revised form
5 May 2011
Accepted 10 May 2011

Keywords:
Vortex-induced vibrations
Mono- and multi-frequency responses
In-line/cross-flow response synchronization
Lock-in in shear flow
Tensioned beam
Direct numerical simulation

ABSTRACT

The mono-frequency as well as multi-frequency vortex-induced vibrations of a tensioned beam of aspect ratio 200, immersed in a linear shear flow at Reynolds number 330 and free to move in both the in-line and cross-flow directions, are studied by means of direct numerical simulation. The structural responses are composed of mixed standing–traveling wave patterns. We observe a switch between mono- and multi-frequency vibrations when the mass ratio changes from a value of 3 to 6, while keeping constant the non-dimensional cable and beam phase velocities. This switch is attributed to the accompanying change in the time-averaged in-line curvature of the beam, which alters the oncoming flow velocity component normal to the structure configuration. It is shown, in general, that the mono- or multi-frequency nature of the response is controlled by the form of the profile of the normal component of the oncoming flow.

Mono- and multi-frequency vibrations may occur in both the in-line and cross-flow directions, with a frequency ratio close to 2. Each excited frequency is associated with a single structural wavenumber. The local synchronization between the vortex shedding and the cross-flow oscillation, i.e. the lock-in condition, occurs in the high velocity zone and covers a similar spanwise extent in both the mono- and multi-frequency cases. Counter-clockwise figure-eight trajectories are very likely to occur within the lock-in region. In both the mono- and multi-frequency types of response, the flow excites the structural vibrations within the lock-in region and damps the structural motions in the non-lock-in region. The multi-frequency character of the response impacts both the lock-in phenomenon and the fluid–structure energy transfer.

1. Introduction

Vortex shedding in the wake of a bluff body immersed in a cross-flow induces unsteady forces on the body, and can lead to vibrations if the body is flexible or flexibly mounted. The phenomenon of vortex-induced vibrations (VIV) occurs in a number of physical problems, especially in the context of long flexible cylindrical structures employed in ocean engineering, such as risers and hawsers. The case of a rigid circular cylinder free to move, or forced to oscillate in the cross-flow direction within a uniform current, is considered as the canonical problem to investigate VIV mechanisms (Bearman, 1984; Sarpkaya, 2004; Williamson and Govardhan, 2004). It has been shown that self-excited, self-limited, large amplitude

* Corresponding author.
E-mail address: bourguet@mit.edu (R. Bourguet).

0889-9746/$ - see front matter © 2011 Elsevier Ltd. All rights reserved.
doi:10.1016/j.jfluidstructs.2011.05.008

oscillations occur when the vortex shedding and the structural vibration frequencies coincide, a condition referred to as 'lock-in'. More recently, some differences have been reported when the rigid cylinder is also allowed to move in the in-line direction (Jauvtis and Williamson, 2004; Jeon and Gharib, 2001; Sarpkaya, 1995). Jauvtis and Williamson (2004) have noticed a dramatic change in the cross-flow response as significant in-line motion appears, as the structure to displaced fluid mass ratio is reduced below 6. An increase in the in-line to cross-flow natural frequency ratio induces changes as well, causing a larger cross-flow peak amplitude response, together with a shift of the lock-in range toward higher reduced velocities (Dahl et al., 2006; Lucor and Triantafyllou, 2008). Furthermore, the orientation and shape of the in-line/cross-flow trajectories can promote higher harmonic fluid forces (Dahl et al., 2007, 2010).

Investigations of flexible cylinders immersed in non-uniform currents have highlighted the increased complexity of the VIV phenomenon (e.g. Chaplin et al., 2005; Lie and Kaasen, 2006; Modarres-Sadeghi et al., 2010; Trim et al., 2005; Vandiver et al., 2009). In shear flow, flexible structure vibrations are often composed of mixtures of standing and traveling wave patterns (Bourguet et al., 2011; Lucor et al., 2006; Newman and Karniadakis, 1997). Contrary to the case of a rigid cylinder, the phase difference between the in-line and cross-flow displacements of a flexible cylinder can vary along the span, leading to diverse trajectories (Modarres-Sadeghi et al., 2010; Vandiver et al., 2009). For a long flexible cylinder freely vibrating in the cross-flow direction and in both the in-line and cross-flow directions, in linear shear flow, Lucor et al. (2001) and Bourguet et al. (2011) reported the occurrence of the lock-in condition only over a portion of the span. The partial occurrence of the 'wake capture' phenomenon (Sarpkaya, 2004) had also been observed in the case of the forced oscillations of a cable in shear flow (Peltzer and Rooney, 1985). Uniform flows induce narrow band excitations often limited to a single vortex shedding frequency. In contrast, non-uniform flows can potentially trigger broad band responses since the Strouhal frequency, i.e. the vortex shedding frequency observed past a stationary cylinder in uniform flow, depends on the oncoming flow velocity. The occurrence of vibrations at several frequencies in non-uniform currents has been emphasized in Kim et al. (1986), Vandiver et al. (1996), Chaplin et al. (2005) and Lucor et al. (2006), for example. Vandiver et al. (1996) have underlined the possible influence of the flow shear rate on the development of responses at a single or multiple frequencies. However, the causes of a switch between these two types of response are still unclear. In addition, the impact of the mono- or multi-frequency content of the vibrations on the lock-in phenomenon and on the fluid–structure energy transfer still needs to be elucidated.

In the present study, direct numerical simulation (DNS) is employed to investigate the mono- and multi-frequency vibrations of a tensioned beam of aspect ratio 200, immersed in a linear shear flow at Reynolds number 330, based on the maximum inflow velocity, and free to move in both the in-line and cross-flow directions. This work aims at characterizing precisely the two types of response, at identifying the reasons of the observed change in the nature of the vibrations and at quantifying the influence of the response nature on the principal fluid–structure interaction mechanisms.

The paper is organized as follows. The coupled fluid–structure model and the numerical method are presented in Section 2. The mono- and multi-frequency structural vibrations are analyzed in Section 3. The causes of the switch between mono- and multi-frequency responses in the present configuration are investigated in Section 4. The impact of the vibration nature on fluid–structure interaction phenomena is examined in Section 5. The findings of the present study are summarized in Section 6.

2. Formulation and numerical method

The tensioned beam under study has a circular cross-section and an aspect ratio $L/D=200$, where L is its length in equilibrium position in quiescent flow and D its diameter. It is pinned at both ends, while it is free to move in both the in-line (x) and cross-flow (y) directions. The beam mass ratio is defined as $m=\rho_c/\rho_f D^2$, where ρ_c is the beam mass per unit length and ρ_f is the fluid density (Newman and Karniadakis, 1997). The actual ratio between the mass of the beam and the mass of the displaced fluid is equal to $m^*=4m/\pi$. Two mass ratios are considered in the present work: a moderate mass ratio, $m=6$ ($m^*=7.64$), was chosen in reference to Jauvtis and Williamson's (2004) work, and a lower value, $m=3$ ($m^*=3.82$), closer to the offshore applications, was also considered. In the following, all physical variables are non-dimensionalized using the cylinder diameter D and the maximum inflow velocity U. The constant tension, bending stiffness and damping of the structure are designated by T, EI and K, respectively. The in-line and cross-flow displacements of the cylinder are denoted by ζ_x and ζ_y. The drag and lift coefficients are denoted by C_x and C_y. The structural dynamics are governed by the following tensioned beam model, expressed in non-dimensional form (Evangelinos and Karniadakis, 1999; Newman and Karniadakis, 1997):

$$\frac{\partial^2 \boldsymbol{\zeta}}{\delta t^2}-\omega_c^2\frac{\partial^2 \boldsymbol{\zeta}}{\delta z^2}+\omega_b^2\frac{\partial^4 \boldsymbol{\zeta}}{\delta z^4}+\frac{K}{m}\frac{\partial \boldsymbol{\zeta}}{\delta t}=\frac{1}{2}\frac{\boldsymbol{C}}{m}, \tag{1}$$

where $\boldsymbol{\zeta}=[\zeta_x,\zeta_y]^T$ and $\boldsymbol{C}=[C_x,C_y]^T$. t denotes the non-dimensional time variable. ω_c and ω_b are the cable and beam phase velocities, defined by $\omega_c^2=T/m$ and $\omega_b^2=EI/m$, respectively. The structural damping is set equal to zero ($K=0$) to allow maximum amplitude oscillations. A tensioned beam is considered in this study with $\omega_c=4.55$ and $\omega_b=9.09$. When the mass ratio is changed between the values of 3 and 6, T and EI are modified accordingly to keep ω_c and ω_b constant, so that vibrations involving similar high wavenumbers develop in both cases, as shown in Section 3. Such vibrations are representative of configurations encountered in the context of ocean engineering (e.g. Chaplin et al., 2005; Lie and Kaasen, 2006).

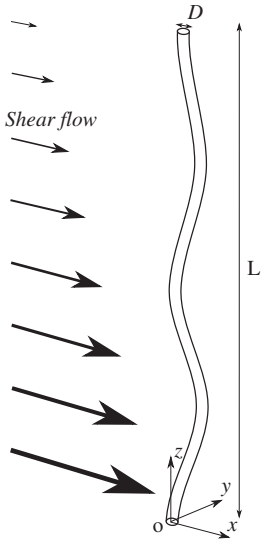

Fig. 1. Sketch of the physical configuration.

The flow is predicted using DNS of the three-dimensional incompressible Navier–Stokes equations. The beam is submitted to an oncoming current which is parallel to the x-axis and linearly sheared along the z-axis, as illustrated in Fig. 1. The maximum inflow velocity U occurs at $z=0$. The ratio between maximum and minimum inflow velocity is equal to 3.67. The Reynolds number (Re) based on D and the inflow velocity ranges from 330 to 90.

The parallelized code *Nektar*, based on the spectral/*hp* element method (Karniadakis and Sherwin, 1999), is used to solve the coupled fluid–structure system. Details regarding validation studies of the numerical method and parameters have been reported in Newman and Karniadakis (1997) and Evangelinos and Karniadakis (1999). The computational domain extends 50D downstream, and 20D upstream, above, and below the cylinder. A two-dimensional grid of 2175 elements with Jacobi polynomials of order $p=7$ is used in the (x,y) planes. In the z-direction, 1024 planes (512 complex Fourier modes) are used. The spatial resolution is similar to Evangelinos and Karniadakis's (1999) study for a cylinder of aspect ratio $L/D=4\pi$ constrained to oscillate in the cross-flow direction, at $\mathrm{Re}=1000$.

Fourier expansion implies spanwise periodicity of the imposed shear velocity profile. The periodicity condition is enforced in a buffer region where the inflow velocity profile is represented by a third-order polynomial that ensures continuity of the velocity profile and its slope. The size of the buffer region, Δz, is chosen equal to 8% of the cylinder length ($\Delta z=16$), in agreement with the recommendations of Lucor et al. (2006). Details concerning buffer region implementation and validation have been reported in Bourguet et al. (2011). In particular, simulations performed with $\Delta z=11$ and 21 have shown the negligible influence of the buffer region size on the rest of the domain, as long as it remains small compared to the cylinder length. As an example, the relative difference on the maximum RMS values of the structure displacements along the span was smaller than 3% between $\Delta z=11$ and 21 cases.

The analysis reported in the present study is based on the monitoring of time series of more than 300 convective time units, collected after the initial transient dies out, with a non-dimensional sampling frequency equal to 40.

3. Mono- and multi-frequency responses

The in-line and cross-flow vortex-induced vibrations of the structure are studied in this section with an emphasis on the frequency content of the structural responses. In the present configuration, a change in the mass ratio causes a change of the time-averaged in-line bending of the beam. The link between the modification of the curvature of the structure and the nature of the responses is investigated in Section 4.

Selected time series of the in-line and cross-flow displacements are presented along the beam span in Fig. 2. In these plots and in the following, only the deviations of the in-line displacement from its mean value, $\tilde{\zeta}_x$, are shown. In both directions and for both mass ratios, the structural responses are mixtures of standing and traveling wave patterns. The traveling components of the vibrations are more pronounced in the in-line direction and principally oriented from the high to low inflow velocity regions (increasing z). Standing wave patterns dominate the region near $z=0$ in both directions until approximately $z=30$. It can be noted that the standing wave component is more pronounced in this region for $m=3$, especially in the in-line direction. Beyond this region, distinct traveling waves are observed; these waves are less altered by the underlying standing wave patterns for $m=3$.

Maximum and root-mean-square (RMS) values of the displacements along the beam span are plotted in Fig. 3. These plots reflect the mixed standing–traveling wave patterns of the responses. The standing character of the vibrations leads to

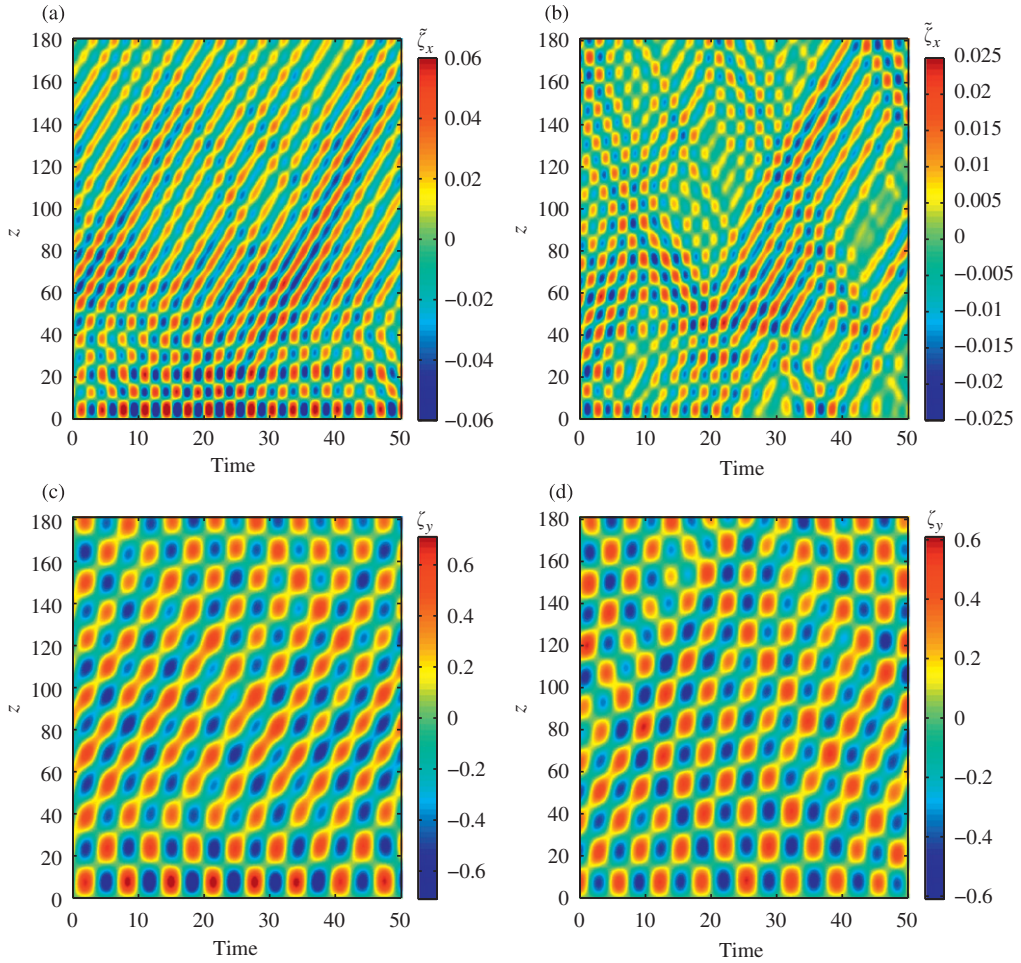

Fig. 2. Selected time series of (a,b) in-line displacement fluctuation and (c,d) cross-flow displacement along the beam span, for (a,c) $m=3$ and (b,d) $m=6$.

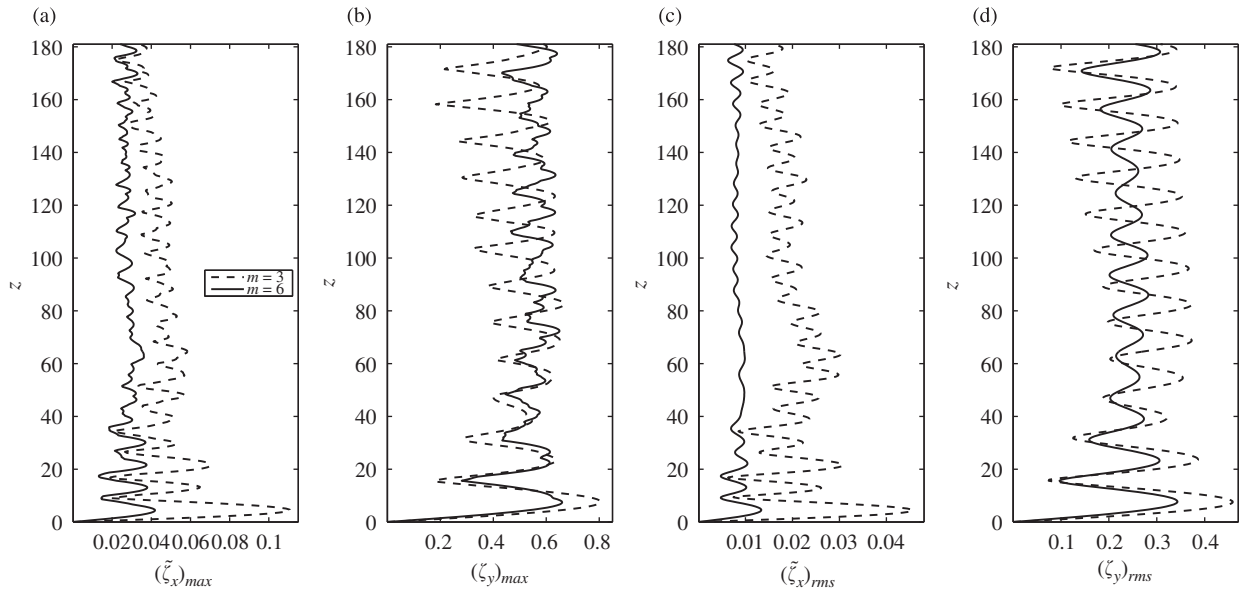

Fig. 3. (a,b) Maximum and (c,d) RMS values of (a,c) in-line displacement fluctuation and (b,d) cross-flow displacement, along the beam span.

the formation of cells along the span corresponding to alternating 'nodes' (minima of the response envelope) and 'anti-nodes' (maxima of the response envelope). The standing character is more pronounced near the ends and especially near $z=0$, as previously observed. The RMS values of displacements associated with nodes are different from zero which emphasizes the modulation of the standing wave patterns by the superimposed traveling wave components. On average (RMS values), larger vibration amplitudes are observed for $m=3$ than for $m=6$. The maximum amplitudes of the cross-flow vibrations are, however, very close. In addition, it is interesting to notice that the amplitude between adjacent node and anti-node is generally smaller for $m=6$. The existence of several excited structural wavenumbers in this case is responsible for this phenomenon as shown in the following on the basis of spectral analysis.

Spatio-temporal spectral analysis is carried out to clarify the nature of the structural vibrations. This is achieved by a two-dimensional FFT of the spatio-temporal evolution of the structural responses which are zero padded to reach a frequency resolution of 5×10^{-4} in both time and space. In Fig. 4, power spectral densities (PSD) of the in-line and cross-flow displacements are plotted as functions of frequency and spatial wavenumber. Positive frequencies are presented and thus negative wavenumbers (upper part of each plot) are associated with traveling waves moving toward the low velocity region while positive wavenumbers (lower part of each plot) represent traveling waves moving toward the high velocity region. PSD are normalized by the maximum observed on both domains (positive and negative wavenumbers) to illustrate the traveling or standing character of the response. The predominant vibration frequencies are identified by yellow vertical dashed lines. Sine Fourier modes ($\sin(\pi nzD/L)$ for the nth mode) are often used to describe the structural response (e.g. Chaplin et al., 2005; Lie and Kaasen, 2006). For illustration purposes, and comparison with the existing literature, the wavenumbers corresponding to selected sine Fourier modes are indicated by white horizontal dashed lines.

A substantial difference exists in the spectral content of the structural responses between the two different mass ratio cases under study: responses at a single frequency are observed in both directions for $m=3$, while the case of $m=6$

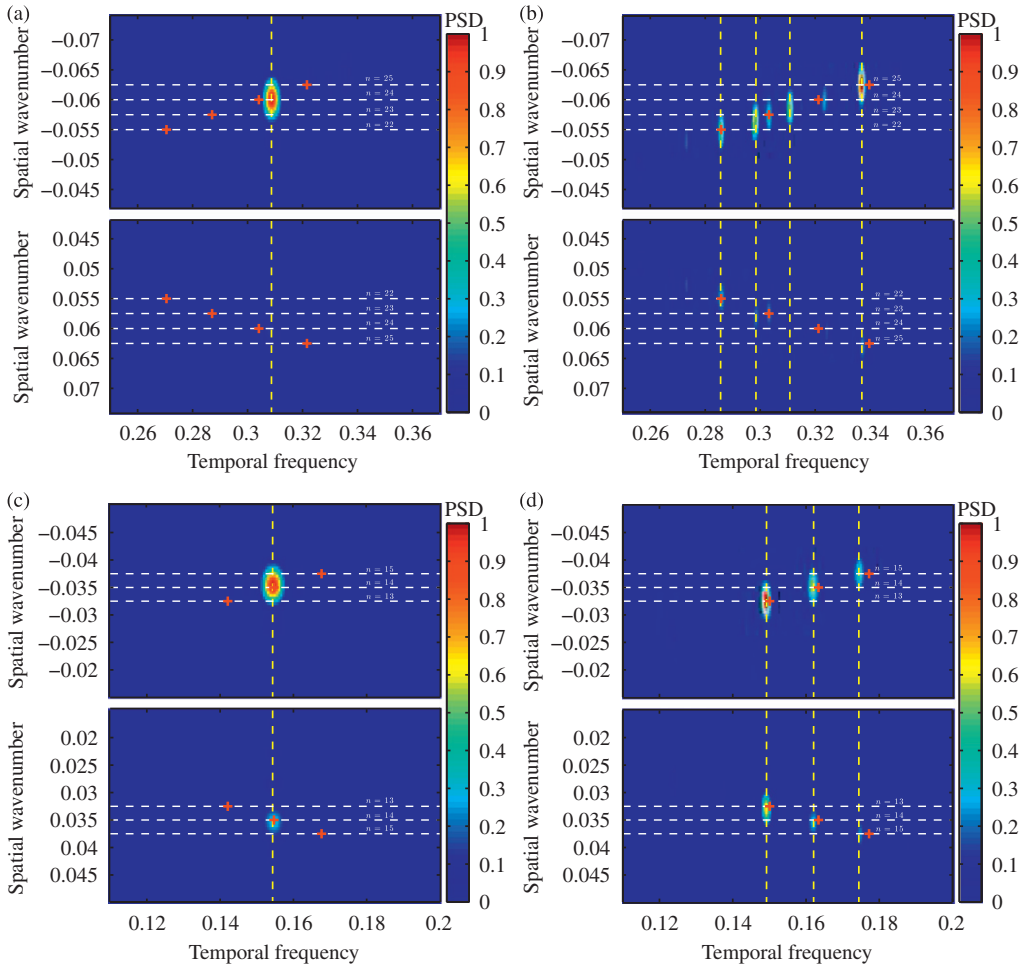

Fig. 4. Spatio-temporal spectral analysis of (a,b) in-line displacement fluctuation and (c,d) cross-flow displacement for (a,c) $m=3$ and (b,d) $m=6$. Yellow vertical dashed lines indicate predominant vibration frequencies. Wavenumbers of selected sine Fourier modes are indicated by white horizontal dashed lines. Red crosses denote the modified natural frequencies of these modes f^{mod} (3). (For interpretation of the references to color in this figure legend, the reader is referred to the web version of this article.)

exhibits responses at several frequencies. These two types of response are referred to as mono-frequency and multi-frequency, respectively. In the case of multi-frequency responses ($m=6$), for instance in the in-line direction, it can be noticed that the frequency peaks are clearly defined and distinct from each other. The ratio between the in-line and cross-flow excited frequencies is close to 2 in both cases. The synchronization between the in-line and cross-flow vibrations is analyzed in Section 5.1.

The predominant excited wavenumbers correspond to modes $n=24$ in the in-line direction and $n=14$ in the cross-flow direction for $m=3$ and $n \in \{22,23,24,25\}$ in the in-line direction and $n \in \{13,14,15\}$ in the cross-flow direction for $m=6$. These mode numbers are close to those measured experimentally by Trim et al. (2005) and Lie and Kaasen (2006), where cases of multi-frequency responses have been reported in shear flow. In the present case of mixed standing–traveling wave responses, it is recalled that the concept of structural modes and the association of the excited wavenumbers with sine Fourier mode numbers are used loosely, for illustration purposes only.

At a given vibration frequency, it appears that only one peak emerges on the spatial spectrum at the same wavenumber on both negative and positive sides, i.e. only one structural wavenumber is excited at a given frequency. The natural frequency f^{nat} of the tensioned beam associated with the wavenumber k can be evaluated as follows, in vacuum:

$$f^{\mathrm{nat}} = k\sqrt{\omega_c^2 + 4\pi^2\omega_b^2 k^2}. \tag{2}$$

This spectrum may be modified to take into account of the immersion of the cylinder into the fluid:

$$f^{\mathrm{mod}} = f^{\mathrm{nat}}\sqrt{\frac{m}{m+\frac{\pi}{4}C_m}}, \tag{3}$$

where C_m is the added mass coefficient induced by the flow. The corresponding modified frequencies, for a choice of $C_m=1$, are indicated by red crosses in Fig. 4. While this modified spectrum provides a reasonable approximation of the effective excited frequencies in some cases, significant deviations appear in other cases (e.g. in-line direction for $m=3$) emphasizing the strong variability of the added mass coefficient.

The relative weights of negative and positive wavenumber peaks for the same frequency provide information concerning the standing/traveling character of the corresponding wave. In all cases, negative peaks dominate, indicating predominant traveling waves moving from the high to low velocity regions (increasing z), as qualitatively observed on the spatio-temporal evolutions plotted in Fig. 2. The ratio between the negative and positive peak amplitudes, for a given frequency, is generally larger for $m=3$. This is in agreement with the previous remark concerning the occurrence of purer, reinforced traveling waves in this case on most of the beam length ($z>30$, approximately).

The causes of the observed switch between mono- and multi-frequency responses as the mass ratio is increased are examined in the next section.

4. Impact of the structural average curvature on the response frequency content

The time-averaged in-line displacement of the beam along its span is presented in Fig. 5(a). As expected from expression (1), since ω_c and ω_b are kept constant, the beam time-averaged curvature increases as the mass ratio is reduced. In both mass ratio cases, the beam exhibits an asymmetric deformation due to the shear flow, with a maximum displacement located near $z=80$. Such asymmetric deformation has been observed experimentally by Chaplin et al. (2005) for a cylinder submitted to a stepped current, for example.

The in-line bending modifies the oncoming flow velocity component normal to the beam. The spanwise evolution of the inflow normal component is plotted in Fig. 5(b) and (c), for $m=3$ and 6, respectively (plain lines). The larger bending observed for $m=3$ induces a stronger deviation of the normal velocity profile from the total, linearly sheared inflow parallel to the x-axis (dotted lines), principally in the high velocity region, for $z<60$ approximately.

To establish that it is the normal velocity profile that determines the mono- or multi-frequency nature of the response, two additional simulations have been performed: (i) a simulation for $m=3$ with a modified sheared inflow profile that emulates the normal velocity profile observed in the case of $m=6$, (ii) a simulation for $m=6$ with a modified sheared inflow profile that emulates the normal velocity profile observed in the case of $m=3$. The profiles of the inflow velocity component normal to the beam reached in these additional simulations are very close to the original ones, as illustrated in Fig. 5(b) and (c) (dashed lines).

The influence of the normal inflow profile is quantified through spectral analysis. The spanwise distributions of the temporal PSD of the cross-flow vibrations are plotted in Fig. 6 for the original and modified inflow cases. PSD is normalized at each spanwise location by the corresponding displacement variance. The mono-frequency nature of the response for $m=3$, when the cylinder is submitted to the original linear shear profile, is confirmed in Fig. 6(a). When the inflow velocity is modified to emulate the normal profile corresponding to the original case of $m=6$ (Fig. 6(b)), the beam exhibits a multi-frequency vibration similar to the original multi-frequency case, with three distinct excited frequencies. Conversely, the original multi-frequency case for $m=6$ (Fig. 6(c)) becomes mainly mono-frequency if the inflow velocity is tuned to match the normal profile observed in the original case of $m=3$ (Fig. 6(d)). Similar changes in the response frequency content are noted in the in-line direction, when the normal velocity profile is modified.

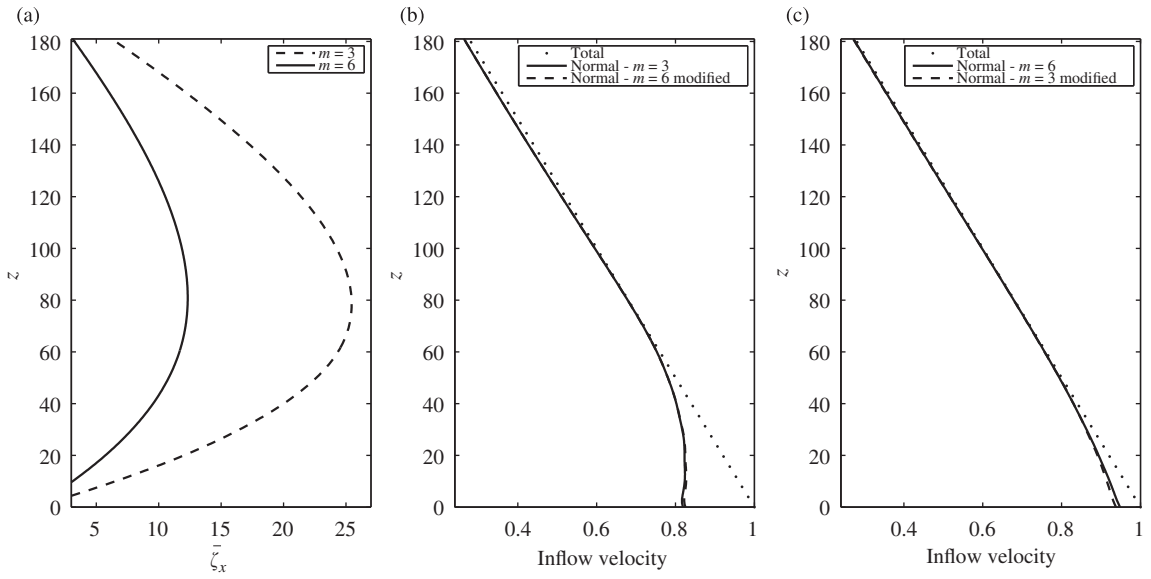

Fig. 5. (a) Time-averaged in-line displacement, (b,c) total and normal inflow velocity profile, along the beam span.

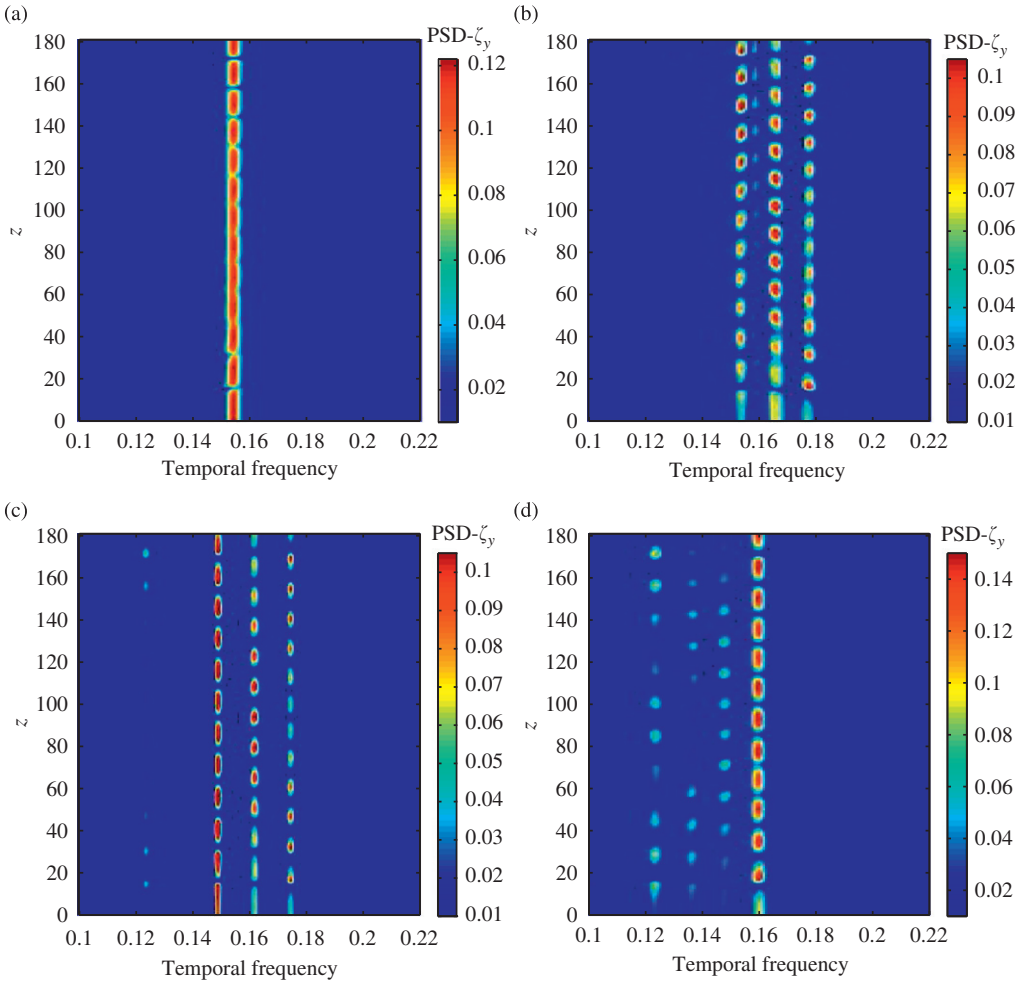

Fig. 6. PSD of the cross-flow displacement along the beam span for (a) $m=3$, (b) $m=3$ with modified inflow profile emulating $m=6$ normal velocity profile, (c) $m=6$, (d) $m=6$ with modified inflow profile emulating $m=3$ normal velocity profile.

Therefore, the observed switch between mono- and multi-frequency vibrations is triggered by the modification of the inflow velocity component normal to the beam. The importance of the normal inflow component has been previously highlighted in the literature, for example through the independence principle (IP) which states that the flow past a yawed cylinder can be compared to the normal incidence case by considering the component of the oncoming flow velocity normal to the cylinder (Schlichting, 1968). The IP is subject, however, to a number of limitations that have been emphasized for stationary and freely vibrating rigid cylinders (e.g. Lucor and Karniadakis, 2003; Ramberg, 1983; Van Atta, 1968).

In the present case, the range of normal velocity in the high velocity region seems to control the vibrational response bandwidth. Specifically, the reduction of this range, as static curvature increases, leads to a narrower excitation bandwidth resulting in mono-frequency response. The role of the high velocity zone in structure excitation is examined in Section 5.3.

5. Influence of the mono-/multi-frequency nature of the vibrations on VIV mechanisms

The above analysis shows that a flexible cylinder in shear flow may exhibit both mono- and multi-frequency responses along the span. The impact of the response mono-/multi-frequency nature on some fluid–structure interaction mechanisms is investigated in this section.

5.1. Synchronization of the in-line and cross-flow vibrations

In Section 3, the in-line and cross-flow responses have been considered separately. They are, in fact, coupled non-linearly through the fluid forces; their synchronization is studied in this section. The spectral analysis above has emphasized that the in-line and cross-flow vibrations mainly occur with a relative frequency ratio of 2. This leads to 'figure-eight' trajectories in the (x,y) plane, as illustrated in Fig. 7(a).

The shape and orientation of the beam trajectories in the (x,y) plane are controlled by the phase difference between the in-line and cross-flow displacements. The instantaneous phases of the in-line and cross-flow displacements (ϕ_x and ϕ_y, respectively) are determined by means of the Hilbert transform. Adopting an approach similar to Huera-Huarte and Bearman (2009), the phase difference Φ_{xy} is evaluated as follows:

$$\Phi_{xy} = [p\phi_x - q\phi_y, \text{ mod } 360^\circ], \tag{4}$$

where p and q are two integer numbers defining the level of synchronization studied. The couple $(p,q)=(1,2)$ is chosen here. Values of Φ_{xy} in the range 0°–180° (180°–360°, respectively) correspond to 'figure-eight' orbits where the beam moves upstream (downstream, respectively) when reaching the cross-flow oscillation maxima. These two types of trajectories are referred to as 'counter-clockwise' and 'clockwise', respectively (Dahl et al., 2007).

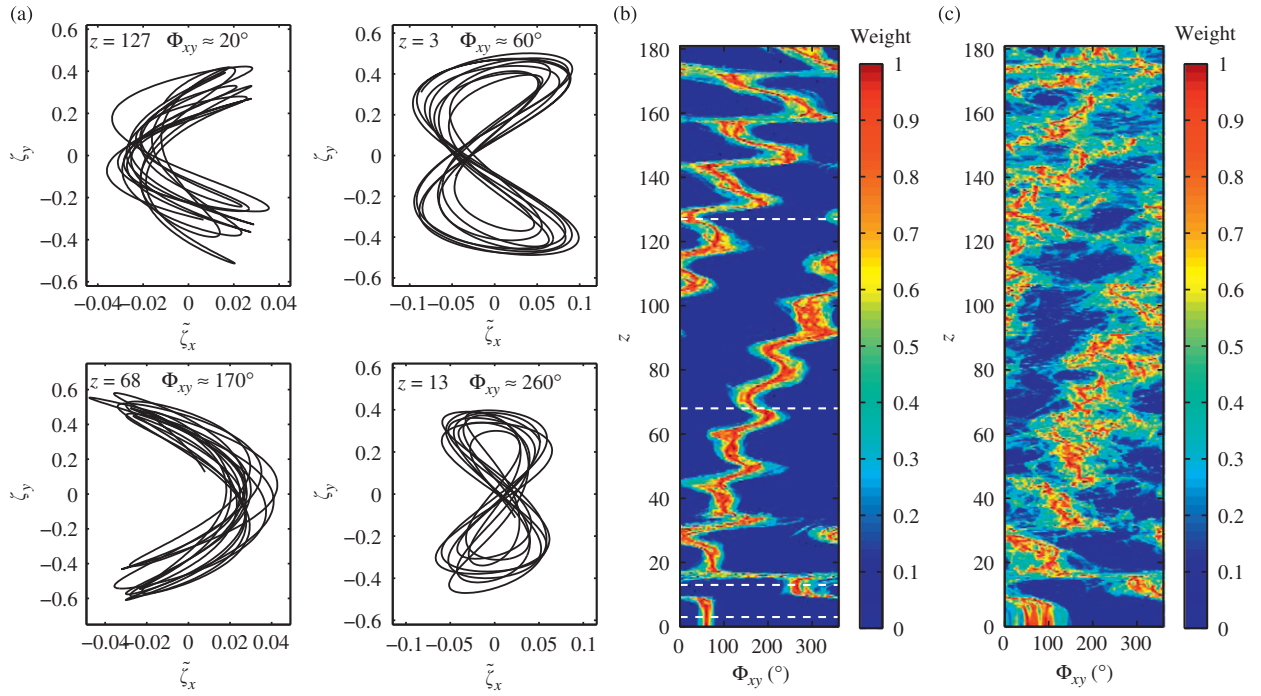

Fig. 7. (a) Selected trajectories of the cylinder at different spanwise locations, for $m=3$. Histogram of phase difference between the in-line and cross-flow displacements along the beam span for (b) $m=3$ and (c) $m=6$. The spanwise locations selected in (a) are identified by white dashed lines in (b).

Histograms of Φ_{xy} are determined from the response time series. Fig. 7(b) and (c) show at each spanwise location the relative weights of the phase difference angles for $m=3$ and 6, respectively. The contributions are normalized by the maximum weight. In Fig. 7(b), the spanwise locations of the selected trajectories in Fig. 7(a) are indicated by white horizontal dashed lines.

The mono/multi-frequency nature of the response does not substantially modify the in-line/cross-flow motion synchronization. In spite of a noisier character in the case of multi-frequency vibrations, both the mono- and multi-frequency cases exhibit very similar synchronization patterns along the span. For $z<30$, approximately, both the in-line and cross-flow vibrations exhibit pronounced standing wave patterns. As a consequence, switching between counter-clockwise and clockwise trajectories are observed near the nodes of the in-line displacements. Beyond this region, this switching counter-clockwise/clockwise pattern is altered by the development of mainly traveling waves, still modulated by an underlying standing wave component. The fact that the nodes of the standing wave pattern in the cross-flow direction do not necessarily coincide with the in-line displacement nodes also alters the above alternating pattern. While perfect traveling waves in both directions would lead to constant Φ_{xy} along the span (Vandiver et al., 2009), perfect standing waves (with a ratio of 2 between the in-line and cross-flow excited structural wavenumbers) would instead be associated with a switching counter-clockwise/clockwise pattern (as observed near $z=0$). In the present case, due to mixed standing–traveling wave vibrations, Φ_{xy} exhibits a zig-zagging spanwise pattern, drifting toward higher phase difference angles as z increases. In addition, it can be noted that counter-clockwise trajectories dominate within the high velocity region. A similar observation has been reported by Vandiver et al. (2009) and Modarres-Sadeghi et al. (2010) on the basis of experimental measurements involving flexible cylinders in shear flows. As shown in the following, this phenomenon coincides with the occurrence of lock-in in this region.

5.2. Lock-in

For long flexible cylinders in shear flow, the lock-in condition can be defined at each spanwise location by the synchronization of the local vortex shedding frequency with the local cross-flow vibration frequency; otherwise, the condition is referred to as non-lock-in. In the following, the spanwise region which includes all the locally locked-in locations is referred to as the lock-in region and the rest of the span as the non-lock-in region.

The vortex shedding frequency is determined from the temporal power spectrum of the cross-flow component of flow velocity v that has been recorded over the same time interval as the beam displacements, along a spanwise line in the wake, at $(x,y)=(31,0)$ in the case of $m=3$ and $(x,y)=(20,0)$ in the case of $m=6$. The spanwise distribution of v PSD is plotted in Fig. 8(a) and (b) for $m=3$ and 6, respectively. The predominant vibration frequencies previously identified (Fig. 4) are indicated by yellow vertical dashed lines.

In both cases, the lock-in region is found in the high flow velocity region, near $z=0$, and the rest of the span corresponds to the non-lock-in region. In the case of forced cross-flow oscillations of a flexible cylinder in shear flow, Peltzer and Rooney (1985) have emphasized the formation of long ($>40D$) spanwise cells of constant shedding frequency, equal to

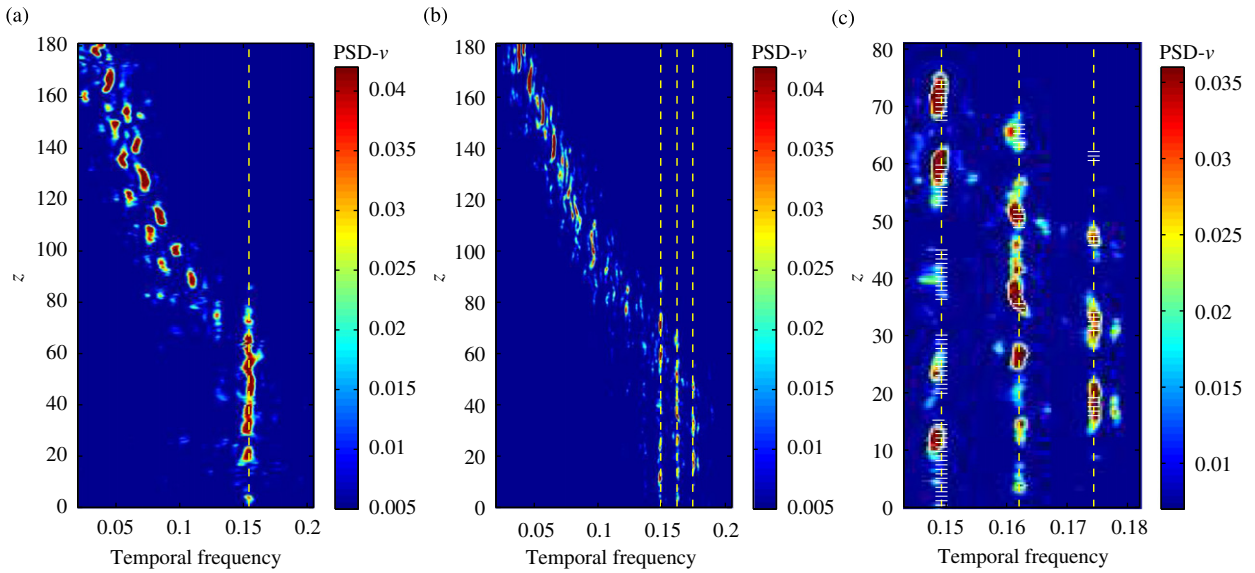

Fig. 8. PSD of the temporal evolution of the cross-flow component of flow velocity along a spanwise line in the wake for (a) $m=3$ and (b) $m=6$. (c) Detail of the lock-in region for $m=6$. Yellow dashed lines indicate the predominant frequencies of the cross-flow vibrations. In (c) white segments denote the local predominant vibration frequency. (For interpretation of the references to color in this figure legend, the reader is referred to the web version of this article.)

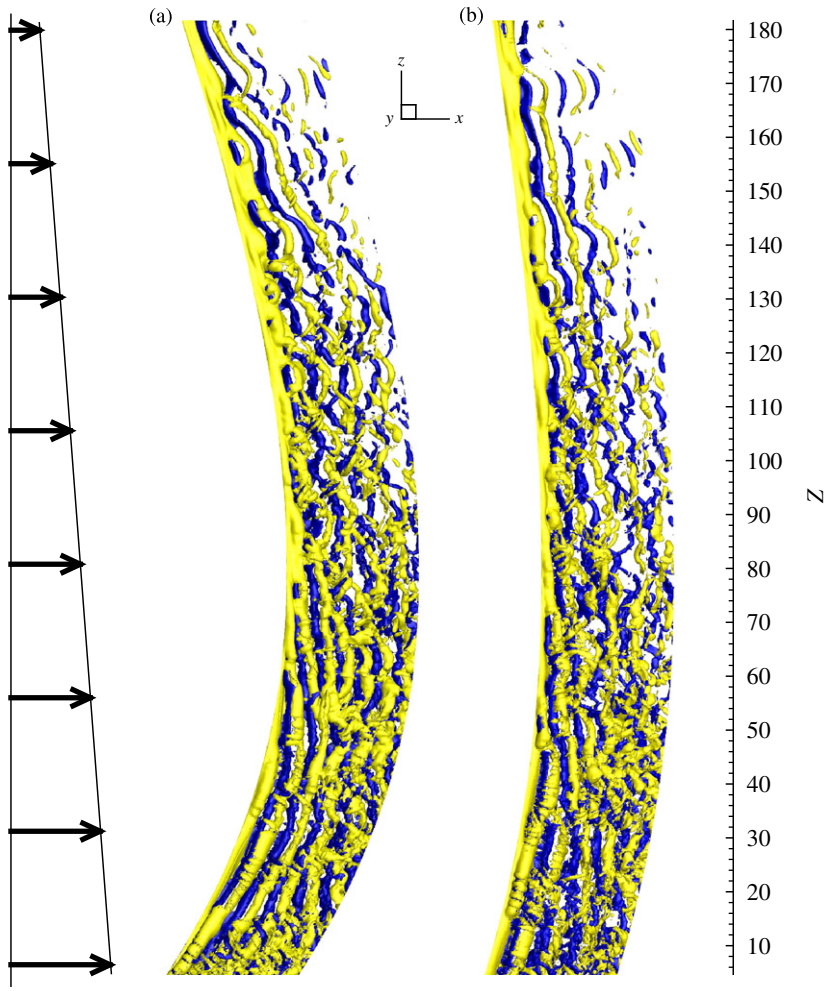

Fig. 9. Instantaneous iso-surfaces of spanwise vorticity ($\omega_z = \pm 0.3$) downstream of the cylinder for (a) $m=3$ and (b) $m=6$. Part of the computational domain is plotted. Arrows represent the linear shear oncoming flow.

the forcing frequency. In the present case of free-vibrations, the spanwise extent of the lock-in region is similar for the mono- and multi-frequency cases, equal to $77D$ for $m=3$ and $75D$ for $m=6$.

The impact of the multi-frequency response is clearly visible within the lock-in region, where lock-in is established at three predominant vibration frequencies. A detailed view of the lock-in region for the multi-frequency case is presented in Fig. 8(c). It is observed that lock-in is generally established at a single frequency at a given spanwise location. The local lock-in frequency often coincides with the local predominant vibration frequency (represented by white segments in Fig. 8(c)). Under lock-in, the vortex shedding frequency may be driven far from the Strouhal frequency observed for a stationary cylinder. Shedding frequencies normalized by the local oncoming flow velocity are in the ranges [0.155,0.22] and [0.15,0.22], for $m=3$ and 6, respectively. The lock-in region occurs in the high velocity zone while the previous observations have shown that counter-clockwise beam trajectories are more likely in this zone; in the lock-in region, the cylinder exhibits principally counter-clockwise orbits.

In both the mono- and multi-frequency cases, the non-lock-in region is characterized by a cellular pattern relatively similar to the case of a stationary cylinder in shear flow, as reported for example in Peltzer and Rooney (1985) for a comparable shear rate.

As in the case of a stationary cylinder in shear flow, or a tapered cylinder in uniform flow (Mukhopadhyay et al., 1999; Piccirillo and Van Atta, 1993), the partitioning of the wake into spanwise cells of constant vortex shedding frequency leads to an oblique orientation of the vortex rows, as illustrated in Fig. 9 by plotting instantaneous iso-surfaces of spanwise vorticity. To ensure the continuity of the spanwise vortex filaments while the vortex shedding frequency is discontinuous, vortex splitting events (e.g. Piccirillo and Van Atta, 1993; Williamson, 1992; Zhang et al., 1995) occur between adjacent cells in Fig. 8. A detailed analysis of the wake patterns occurring in a similar physical configuration, for $m=6$ and various Reynolds numbers, has been reported in Bourguet et al. (2011).

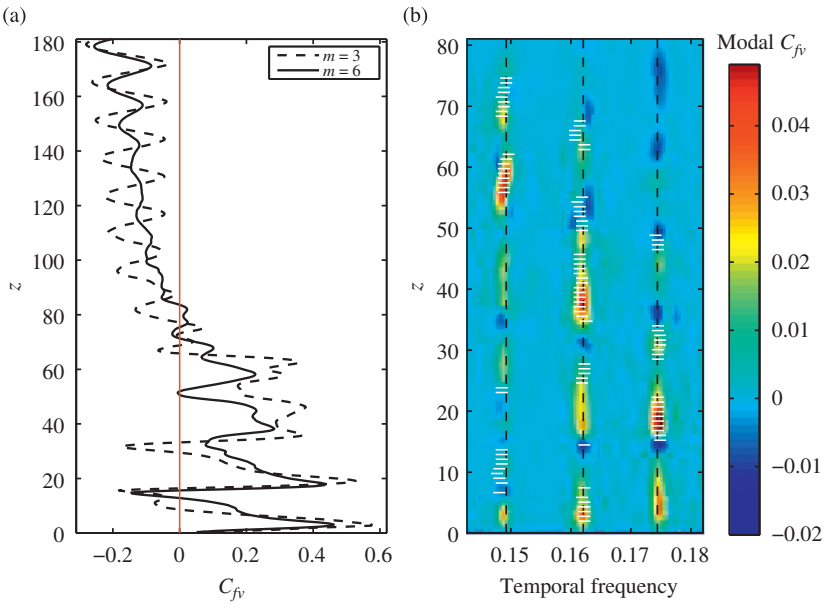

Fig. 10. (a) Spanwise evolution of the time-averaged force coefficient in phase with the beam velocity. (b) Frequency decomposition of the force coefficient in phase with the beam velocity for $m=6$, detail of the lock-in region. In (b) black dashed lines indicate the predominant frequencies of the cross-flow vibration and white segments denote the local lock-in frequency.

5.3. Fluid–structure energy transfer

Fluid–structure energy transfer can be quantified by the fluid force coefficient in phase with the beam velocity (Hover et al., 1998; Newman and Karniadakis, 1997). The time-averaged value of this coefficient, including both the in-line and cross-flow contributions, is defined as:

$$C_{fv} = \frac{\sqrt{2}\langle \tilde{C}_x \dot{\tilde{\zeta}}_x + C_y \dot{\zeta}_y \rangle}{\sqrt{\langle \dot{\tilde{\zeta}}_x^2 + \dot{\zeta}_y^2 \rangle}}, \tag{5}$$

where $\langle \cdot \rangle$ denotes the time-averaging operator and $\tilde{C}_x$ is the fluctuating component of C_x. Positive values of C_{fv} indicate that the fluid supplies, on average, energy to the structure and hence excites the vibrations, while negative values indicate that the fluid is damping the structural motion.

The spanwise evolution of C_{fv} is plotted in Fig. 10(a), for both mass ratio cases. Zones of positive C_{fv} are located on the high velocity side and are contained within the lock-in region. In the non-lock-in region, C_{fv} remains negative. Hence, the vibrations are excited by the flow in the lock-in region and damped in the non-lock-in region. It is important to mention that, in both the mono- and multi-frequency cases, the excitation of the structural vibrations is not uniform within the lock-in region. In particular, C_{fv} tends to decrease in spanwise zones where the beam exhibits clockwise trajectories and negative peaks can occur near the cross-flow vibration nodes.

The reinforced standing wave pattern for approximately $z<30$ in the case of $m=3$ is accompanied by stronger modulations of C_{fv} in the lock-in region. In the case of multi-frequency response, the fluid–structure energy transfer occurs at the three frequencies of lock-in, as illustrated in Fig. 10(b) through a frequency decomposition of C_{fv} within the lock-in region. It can be noted that the flow excites the structural vibrations in this zone principally at the local lock-in frequency (white segments). The three main peaks of positive C_{fv} ($z\approx 18$, $z\approx 38$, $z\approx 57$) indeed occur at the local lock-in frequency.

6. Conclusions

Mono-frequency as well as multi-frequency vortex-induced responses of a long tensioned beam, subject to sheared oncoming cross-flow, have been investigated by means of DNS at Reynolds number 330. The structural responses are found to consist of mixed standing and traveling wave patterns; the in-line and cross-flow vibrations exhibit frequencies with a ratio close to a value of 2. The traveling wave components are mainly oriented from the high to low flow velocity regions. Mono- and multi-frequency vibrations occur in both the in-line and cross-flow directions for the two mass ratios studied, $m=3$ and 6. In both cases of mono- and multi-frequency responses, each excited frequency is associated with a single structural wavenumber.

The switch between mono- and multi-frequency responses is controlled by the profile of the oncoming flow component normal to the beam configuration; hence changes in the in-line static curvature of the structure can trigger a transition from one type of response to the other, since it changes the normal velocity component.

The in-line and the cross-flow responses exhibit a spanwise zig-zagging synchronization pattern for both mono- and multi-frequency responses. Likewise, for both types of response, lock-in occurs in the high velocity zone and covers a similar spanwise extent, and counter-clockwise figure-eight trajectories are very likely to occur within the lock-in region. Also, for mono- and multi-frequency cases, the flow excites the structural vibrations within the lock-in region and damps the structure motions in the non-lock-in region.

For multi-frequency vibrations, lock-in is established with all the observed vibration frequencies. However, lock-in remains a locally mono-frequency event, involving preferentially the locally predominant structural vibration frequency. Structural excitation occurs at multiple frequencies across the lock-in region, but for a given spanwise location, it occurs mainly at a single frequency, the local lock-in frequency.

Acknowledgments

The authors wish to acknowledge support from the BP-MIT Major Projects Programme, monitored by M. Tognarelli and P. Beynet; and the Office of Naval Research under Grants N00014-07-1-0135 and N00014-07-1-0446, monitored by T. Swean, Jr.

References

Bearman, P.W., 1984. Vortex shedding from oscillating bluff bodies. Annual Review of Fluid Mechanics 16, 195–222.
Bourguet, R., Karniadakis, G.E., Triantafyllou, M.S., 2011. Vortex-induced vibrations of a long flexible cylinder in shear flow. Journal of Fluid Mechanics 677, 342–382.
Chaplin, J.R., Bearman, P.W., Huera-Huarte, F.J., Pattenden, R.J., 2005. Laboratory measurements of vortex-induced vibrations of a vertical tension riser in a stepped current. Journal of Fluids and Structures 21, 3–24.
Dahl, J.M., Hover, F.S., Triantafyllou, M.S., 2006. Two-degree-of-freedom vortex-induced vibrations using a force assisted apparatus. Journal of Fluids and Structures 22, 807–818.
Dahl, J.M., Hover, F.S., Triantafyllou, M.S., Dong, S., Karniadakis, G.E., 2007. Resonant vibrations of bluff bodies cause multivortex shedding and high frequency forces. Physical Review Letters 99, 144503.
Dahl, J.M., Hover, F.S., Triantafyllou, M.S., Oakley, O.H., 2010. Dual resonance in vortex-induced vibrations at subcritical and supercritical Reynolds numbers. Journal of Fluid Mechanics 643, 395–424.
Evangelinos, C., Karniadakis, G.E., 1999. Dynamics and flow structures in the turbulent wake of rigid and flexible cylinders subject to vortex-induced vibrations. Journal of Fluid Mechanics 400, 91–124.
Hover, F.S., Techet, A.H., Triantafyllou, M.S., 1998. Forces on oscillating uniform and tapered cylinders in crossflow. Journal of Fluid Mechanics 363, 97–114.
Huera-Huarte, F.J., Bearman, P.W., 2009. Wake structures and vortex-induced vibrations of a long flexible cylinder part 1: dynamic response. Journal of Fluids and Structures 25, 969–990.
Jauvtis, N., Williamson, C.H.K., 2004. The effect of two degrees of freedom on vortex-induced vibration at low mass and damping. Journal of Fluid Mechanics 509, 23–62.
Jeon, D., Gharib, M., 2001. On circular cylinders undergoing two-degree-of-freedom forced motions. Journal of Fluids and Structures 15, 533–541.
Karniadakis, G.E., Sherwin, S., 1999. Spectral/hp Element Methods for CFD, first ed. Oxford University Press, Oxford.
Kim, Y.H., Vandiver, J.K., Holler, R., 1986. Vortex-induced vibration and drag coefficients of long cables subjected to sheared flow. ASME Journal of Energy Resources Technology 108, 77–83.
Lie, H., Kaasen, K.E., 2006. Modal analysis of measurements from a large-scale VIV model test of a riser in linearly sheared flow. Journal of Fluids and Structures 22, 557–575.
Lucor, D., Imas, L., Karniadakis, G.E., 2001. Vortex dislocations and force distribution of long flexible cylinders subjected to sheared flows. Journal of Fluids and Structures 15, 641–650.
Lucor, D., Karniadakis, G.E., 2003. Effects of oblique inflow in vortex-induced vibrations. Flow, Turbulence and Combustion 71, 375–389.
Lucor, D., Mukundan, H., Triantafyllou, M.S., 2006. Riser modal identification in CFD and full-scale experiments. Journal of Fluids and Structures 22, 905–917.
Lucor, D., Triantafyllou, M.S., 2008. Parametric study of a two degree-of-freedom cylinder subject to vortex-induced vibrations. Journal of Fluids and Structures 24, 1284–1293.
Modarres-Sadeghi, Y., Mukundan, H., Dahl, J.M., Hover, F.S., Triantafyllou, M.S., 2010. The effect of higher harmonic forces on fatigue life of marine risers. Journal of Sound and Vibration 329, 43–55.
Mukhopadhyay, A., Venugopal, P., Vanka, S.P., 1999. Numerical study of vortex shedding from a circular cylinder in linear shear flow. Journal of Fluids Engineering 121, 460–468.
Newman, D.J., Karniadakis, G.E., 1997. A direct numerical simulation study of flow past a freely vibrating cable. Journal of Fluid Mechanics 344, 95–136.
Peltzer, R.D., Rooney, D.M., 1985. Vortex shedding in a linear shear flow from a vibrating marine cable with attached bluff bodies. Journal of Fluids Engineering 107, 61–66.
Piccirillo, P.S., Van Atta, C.W., 1993. An experimental study of vortex shedding behind linearly tapered cylinders at low Reynolds number. Journal of Fluid Mechanics 246, 163–195.
Ramberg, S.E., 1983. The effects of yaw and finite length upon the vortex wakes of stationary and vibrating circular cylinders. Journal of Fluid Mechanics 128, 81–107.
Sarpkaya, T., 1995. Hydrodynamic damping, flow-induced oscillations, and biharmonic response. Journal of Offshore Mechanics and Arctic Engineering 117, 232–238.
Sarpkaya, T., 2004. A critical review of the intrinsic nature of vortex-induced vibrations. Journal of Fluids and Structures 19, 389–447.
Schlichting, H., 1968. Boundary Layer Theory, sixth ed. McGraw-Hill, New York.
Trim, A.D., Braaten, H., Lie, H., Tognarelli, M.A., 2005. Experimental investigation of vortex-induced vibration of long marine risers. Journal of Fluids and Structures 21, 335–361.
Van Atta, C.W., 1968. Experiments on vortex shedding from yawed circular cylinders. AIAA Journal 6, 931–933.
Vandiver, J.K., Allen, D., Li, L., 1996. The occurrence of lock-in under highly sheared conditions. Journal of Fluids and Structures 10, 555–561.

Vandiver, J.K., Jaiswal, V., Jhingran, V., 2009. Insights on vortex-induced, traveling waves on long risers. Journal of Fluids and Structures 25, 641–653.
Williamson, C.H.K., 1992. The natural and forced formation of spot-like 'vortex dislocations' in the transition of a wake. Journal of Fluid Mechanics 243, 393–441.
Williamson, C.H.K., Govardhan, R., 2004. Vortex-induced vibrations. Annual Review of Fluid Mechanics 36, 413–455.
Zhang, H.Q., Fey, U., Noack, B.R., Konig, M., Eckelmann, H., 1995. On the transition of the cylinder wake. Physics of Fluids 7, 779–794.